ESC HEART FAILURE
ESC Heart Failure 2017; **4**: 331–340
Published online 12 March 2017 in Wiley Online Library (wileyonlinelibrary.com) **DOI:** 10.1002/ehf2.12140

ORIGINAL RESEARCH ARTICLE

The neuroprotective agent Rasagiline mesylate attenuates cardiac remodeling after experimental myocardial infarction

Aimilia Varela[1*†], Manolis Mavroidis[2†], Michalis Katsimpoulas[1], Irini Sfiroera[2], Niki Kappa[2], Angelica Mesa[1], Nikolaos G. Kostomitsopoulos[1] and Dennis V. Cokkinos[1]

[1]*Clinical, Experimental Surgery and Translational Research Center, Athens, Greece;* [2]*Basic Research Center, Biomedical Research Foundation Academy of Athens (BRFAA), Athens, Greece*

Abstract

Aim Rasagiline mesylate (N-propargyl-1 (R)-aminoindan) (RG) is a selective, potent irreversible inhibitor of monoamine oxidase-B with cardioprotective and anti-apoptotic properties. We investigated whether it could be cardioprotective in a rat model undergoing experimental myocardial infarction (MI) by permanent ligation of the left anterior descending coronary artery.

Methods and results RG was administered, intraperitoneally, for 28 days (2 mg/kg) starting 24 h after MI induction. Echocardiography analysis revealed a significant reduction in left ventricular end-systolic and diastolic dimensions and preserved fractional shortening in RG-treated compared with normal saline group at 28 days post-MI (31.6 ± 2.3 vs. 19.6 ± 1.8, $P < 0.0001$), respectively. Treatment with RG prevented tissue fibrosis as indicated by interstitial collagen estimation by immunofluorescence staining and hydroxyproline content and attenuated the number of apoptotic myocytes in the border zone (65%) as indicated by terminal deoxynucleotidyl transferase dUTP nick end labeling (TUNEL) assay. Caspase 3 relative protein levels were significantly decreased in the non-infarcted myocardium. Markedly decreased malondialdehyde levels in the border zone indicate a reduction in tissue oxidative stress.

Conclusions Our study demonstrates a positive effect of RG in the post-MI period with a significant attenuation in cardiac remodelling.

Keywords Rasagiline mesylate; Myocardial infarction; Cardiac remodelling; Fibrosis; Apoptosis

Received: 30 June 2016; Revised: 21 December 2016; Accepted: 10 January 2017
**Correspondence to: Aimilia Varela, BRFAA, 4 Soranou Effesiou St, 11527 Athens, Greece. Tel: + 0030 2106597390. Email: evarela@bioacademy.gr*
†These authors contributed equally to this work.

Introduction

Myocardial infarction (MI) remains one of the most dramatic presentations of coronary artery disease with left ventricular remodeling (LVR) being a significant factor of post-MI prognosis.[1] LVR is a process of gradual cardiac enlargement, dysfunction, and typical molecular changes such as increased cell death, collagen accumulation, and oxidative stress. Cell death is the 'primum movens' of the process.[2] New insights in the pathobiology of myocardial ischemic injury suggest that myocyte loss during the acute stage involves both apoptotic and non-apoptotic cell death, thus enabling the development of new pharmacological agents.[3] Monoamine oxidase (MAO) inhibitors have been shown to be effective against myocardial ischemia/reperfusion injury.[4] In the present study, we investigated Rasagiline mesylate (RG) effects in LVR after a permanent ligation MI model. This experimental model permits the long-term study of the LVR as previously described.[5,6]

RG is a potent, selective, irreversible monoamine oxidase-B (MAO-B) inhibitor, developed to prolong the action of dopamine in the brain[7] and is an FDA-approved drug, used to treat Parkinson's disease. It has neuroprotective and anti-apoptotic properties in a variety of *in vitro* and *in vivo* animal models relevant to Parkinson's disease.[8–11] RG can rescue degenerating dopamine neurons through inhibiting death signal transduction initiated by the mitochondria permeability

transition pore.[12] Kleiner *et al.*[13] reported the potential cardioprotective property of the S-isomer of RG, TVP1022, a non-MAO B inhibitor, in neonatal rat ventricular myocyte cultures, with attenuation of doxorubicin cardiotoxicity, manifested by inhibition of cleaved caspase 3 levels increase and reversal of the decline of Bcl-2/Bax ratio. More recent studies demonstrated that TVP1022 attenuated cardiac remodelling and kidney dysfunction in an experimental volume overload-induced congestive heart failure model[14] and preserved mitochondrial integrity via activation of the PKC/GSK-3β pathway in a rat model of ischemia/reperfusion injury, when given before induction of ischemia.[15] Regarding the cardiovascular effects of RG, it has no sympathomimetic activity[16] nor causes significant changes in cardiac hemodynamics.[17]

In view of the major role of apoptosis and oxidative stress in the pathogenesis of cardiac LVR, we investigated the cardioprotective and anti-apoptotic properties of RG in a rat model of permanent MI and long-term LVR.

Methods

Experimental model

Experiments were conducted in 6 month male Wistar rats (350–400 g) maintained in the animal facility of BRFAA. All animals were housed on a 12 h light–dark cycle in a room at a constant temperature (22 ± 1°C), humidity control, and with *ad libitum* access to tap water and standard rodent diet. The investigation conforms to the *Guide for the Care and Use of Laboratory Animals* published by the US National Institutes of Health (NIH Publication No. 85-23, revised 1985) and to the National legal framework (P.D. 56/2013) in harmonization to the *European Directive 63/2010*.[18]

The study included three groups (n = 10 rats per group). Sham: Thoracotomy without MI induction or any treatment, RG: MI and RG, 2.0 mg/kg/day, N/S: MI and normal saline (N/S) 0.9%/day. RG or N/S was administered by intraperitoneal injections,[19,20] for 28 days, beginning 24 h post-MI.

Transthoracic echocardiography

The rats were anesthetized with 1.0% isoflurane by mask and situated in the supine position on a warming pad. The chest was shaved and electrocardiogram limb electrodes were placed. Cardiac function (n = 10 rats per group) was assessed by two-dimensional targeted M-mode echocardiography imaging from the left parasternal short axis view at the level of greatest left ventricular (LV) dimension (Vivid 7, GE, 13 MHz linear transducer), as previously described,[21–24] at the following time intervals: baseline (pre-MI induction), 7, 14 and 28 days post-MI induction. Images were analysed offline using the Echopac PC SW 3.1.3/software (GE). The LV end-diastolic diameter (LVEDD) and LV end systolic diameter (LVESD) were measured. The percentage of LV fractional shortening (FS), FS (%) = [(LVEDD − LVESD) / LVEDD] × 100 was calculated.

Ligation of the left anterior descending coronary artery

MI was induced surgically by a permanent ligation of the left anterior descending (LAD) coronary artery. Surgery was performed under deep isoflurane anesthesia (5% in 0.8lt/min O_2 for induction anesthesia and 3% for intubation and maintenance of anesthesia) determined by total absence of reaction to pain under spontaneous respiration; all efforts were made to minimize suffering of the animals. Left thoracotomy was performed at the fourth intercostal space to expose the heart and LAD coronary artery. A 7-0 polypropylene suture (Prolene, Ethicon, Germany) was then used to ligate permanently the LAD coronary artery, and the incision site was closed using standard surgical techniques with absorbable suture 4/0 (Vicryl, Ethicon, Germany).[25] Electrocardiography was used to demonstrate ST-segment elevation and thereby confirm the success of surgery. The sham group underwent the same surgical procedure without LAD coronary artery occlusion. At the endpoint of the experiment (28th day), the hearts were excised, and the area extending 1.0–2.0 mm from the infarct scar was considered to represent the border zone (BZ), while the rest of the LV was considered to represent the non-infarcted remote myocardium (Remote Region, RR).[26]

Determination of myocardial infarct area (infarct area/area at risk%, I/AAR%)

At the endpoint of the experiment, the hearts (n = 5 rats per group) were excised and stained with Evans Blue, through the aorta, in order to reveal the normally perfused part of the myocardium. Subsequently, 1% triphenyltetrazolium chloride (TTC, in PBS, pH = 7.4) was injected, and the heart was incubated at 37°C for 20 min, in order to determine the ischemic and the infarcted area. After staining, the heart was stored in −80°C and then sliced into 5 mm sections. Evans blue stained (blue staining, non-ischemic area), TTC stained (red staining, ischemic area), and non-TTC stained (white, infarct area) area were analysed. The ischemic region (area at risk) was determined as the percentage of red plus white in relation to the total area (red plus white plus blue). Infarct size was determined as the percentage of white compared with the total area of white plus red as previously described.[27] The nonischemic, ischemic, and infarct regions were quantified

by ImageJ software. Calculations were averaged over all sections from each heart.

Immunofluorescent staining

Frozen tissue sections (10 μm thick) from the three experimental groups 28 days post-MI were fixed with acetone/methanol at −20°C for 20 min and then used for immunolabeling. The anti-desmin monoclonal antibody (1:50 dilution, D33, DAKO Carpinteria, CA) and the anti-collagen-αI polyclonal antibody (1:300 dilution, LF-67, kindly provided by Dr. Larry Fisher, NIH, USA). The appropriate secondary antibodies (conjugated with AlexaFluor-594 and AlexaFluor-488) from Molecular Probes (Leiden, Netherlands), used in 1:1200 dilutions. All the antibodies were incubated in 2% BSA in PBS with 0.1% Tween-20 for 3 h at room temperature. Sections were mounted with fluorescent mounting medium from DAKO (Carpinteria, CA). For confocal imaging, a Leica TCS SP5, DMI6000, microscope (inverted, with the acquisition software LAS-AF, at 23–24°C; Leica Microsystems, Wetzlar, Germany) was used. For the collagen analysis, three sections per animal for the BZ and five sections per animal for the RR were analysed. Each section was 0.5 mm apart and stained with the anti-collagen-αI polyclonal antibody as described above. The extent of collagen content was graded from 0 to 4, according to the amount of red pixels as a percentage of total pixels in the given section (*Figure 2A–C*). Grade 0, 1, 2, 3, and 4 correspond to 0–5%, 5–10%, 10–20%, 20–40% and more than 40% red pixels respectively, as previously described.[21]

Fibrosis assay-hydroxyproline assay

Quantification of myocardial hydroxyproline (HOP) concentrations, an indicator of collagen content, was performed as previously described.[28] Briefly, the tissue was minced, its mass determined, and hydrolyzed overnight in 2 mL of 6 M hydrochloric acid at 110°C. Subsequently, 10 μL hydrolysate was mixed with 150 μL isopropanol, then 75 μL of 1.4% chloramine-T (Sigma, St. Louis, MO) in citrate buffer and oxidized at room temperature for 10 min. One millilitre of Ehrlich's reagent (1.5 g of 4-(dimethylamino) benzaldehyde, 5 mL ethanol, 338 μL sulfuric acid, 15 mL isopropanol) was added and incubated for 30 min at 55°C followed by extinction measurement at 558 nm. From the initial overnight hydrolysate samples, 5 μL was diluted 10 times with 10 mM Tris–HCl, pH = 8.8, and protein concentration was estimated by the Bradford assay (Sigma). Therefore, results were reported as relative HOP absorption values at 558 nm normalized to protein concentration as estimated by Bradford extinction measurement at 595 nm. Measurements of each group were performed in triplicate, and standard deviation was less than ±10%.

Malondialdehyde assay

Lipid peroxide formation was determined by the presence of thiobarbituric acid reactive substances which can be measured colorimetrically, as previously described[29] in RG, N/S, and Sham group (n = 5 rats, per group). Malondialdehyde (MDA), an end product of lipid peroxidation, can be found in most biological samples, is considered as a marker of lipid peroxidation and provides an estimation of oxidative stress.[29,30] Results are expressed as nanomole of MDA per milligram of protein.

Terminal deoxynucleotidyl transferase dUTP nick-end labeling assay

Apoptotic cells were identified by immunofluorescent staining, with terminal deoxynucleotidyl transferase and terminal deoxynucleotidyl trasferase dUTP nick-end labeling (TUNEL) assay, on frozen cardiac tissue sections, as previously described.[21] Briefly, four sections for each heart region (BZ or RR) were analysed by two independent, blinded observers. Each section was 150 to 200 μm apart from the previous one, so a total thickness of 0.6 to 0.8 mm of tissue was analysed. The total number of TUNEL positive nuclei in the given section was counted. The negative control was a serial section in which the terminal transferase enzyme was omitted. The positive control was a DNAse-treated section.

Western blot analysis

Whole tissue protein extracts (RR, BZ, Sham. n = 5 rats per group) were homogenized in extraction buffer containing 10 mM Tris (pH 6.8), 2 mmol/L EDTA, 0.2% SDS, 0.2% DOC, 1 mmol/L Na_3VO_4, 2 mM NaF, 2 mmol/L DTT, 0.5 mmol/L PMSF, and protease inhibitors (Protease Inhibitor Cocktail, Sigma-Aldrich). The homogenates were sonicated and centrifuged for 10 min at 10 000 rpm at 4°C. Protein concentration was determined by the Bradford assay. Total protein lysates (50 μg) were resolved in 10% sodium dodecyl sulphate (SDS)-polyacrylamide gels and transferred to polyvinylidene difluoride (PVDF) membranes (Porablot PVDF membranes, Macherey-Nagel). Membranes were incubated with antibodies directed against: Bcl-2 (1:400 dilution, sc-492, Santa Cruz Biotechnology), Bax (1:400 dilution, sc-7480, Santa Cruz Biotechnology), cleaved Caspase-3 (1:500 dilution, Asp175, Cell Signaling Technology), and glyceraldehyde 3-phosphate dehydrogenase (GAPDH) (1:3000 dilution, AM4300, Applied Biosystems). Band visualization was performed using the enhanced chemiluminescence detection system (ECL, Amersham Biosciences, PA, USA), and quantification was accomplished using the computerized imaging program Quantity One Basic Software (Biorad Laboratories). The values were normalized to GAPDH intensity levels.

Real-time RT-PCR (qRT-PCR)

Total RNA was extracted (RR, BZ, Sham. n = 5 rats per group) using the TRIzol reagent according to the manufacturer's protocol (Life Technologies-Invitrogen). One microgram of total RNA was used to perform reverse transcription and cDNA was generated using the Moloney Murine Leukemia Virus Reverse Transcriptase. Primers used for the PCR produced by Integrated DNA Technologies (Leuven, Belgium) and were for TGF-b1: Sense 5′ GGGCTTTCGCTTCAGTGCT 3′, Antisense 5′ TCGGTTCATGTCATGGATGGT 3′, Collagen I: Sense 5′ TGGTCCTCTGGGCATTGC 3′, Antisense 5′ CACTGCCAGG GTTACCATCA 3′, TIMP-2: Sense 5′ GGAGGAAAGAAGGAATAT CTAATTGCAG 3′, Antisense 5′CCAGGGCACAAT AAAGTCA CAGA 3′, and GAPDH: Sense 5′ CAACTCCCTCAAGA TTGTCAGCAA 3′, Antisense 5′ GGCATGGACTGTGGTCATGA 3′. qRT-PCR was performed using the LightCycler 480 (Roche Mannheim, Germany). Briefly, each 20 μL reaction contained 2 μL cDNA (20 ng of total RNA), each primer at 200 nM and 10 μL of KAPA SYBR FAST qPCR master mix (KAPA BIO, Boston MA, USA). After an initial denaturation step at 95°C for 10 min, the PCR conditions were: 95°C × 30 s, 60°C × 40 s, 72°C × 40 s, 40 cycles. All samples were run in duplicate, and the mean value was used for all further calculations. The $2^{-\Delta\Delta CT}$ method analysis of relative gene expression using qRT-PCR and the 2(−Delta Delta C(T)) method were used to calculate the relative changes in gene expression. All data were normalized by GAPDH levels and expressed as % relative to controls, as previously described.[31]

Statistical analysis

Statistical comparisons were performed using analysis of variance (ANOVA) with Bonferroni/Dunn post-hoc test or the unpaired Student's t-test where appropriate. Data are presented as mean ± SE and were analysed by using Statview 5.0 (Abacus Concepts, SAS Institute, Cary, USA). A $P < 0.05$ value was considered significant. Echocardiography data are

Table 1 LV function echocardiography analysis

	Pre-MI	7 d	14 d	28 d
Sham (n = 10)				
Heart rate	330.66 ± 5.72	329.44 ± 7.09	341.44 ± 8.39	338.18 ± 4.43
LVEDD, mm	7.74 ± 0.19	7.97 ± 0.17	7.97 ± 0.16	7.77 ± 0.15
LVESD, mm	4.52 ± 0.14	4.74 ± 0.09	4.62 ± 0.11	4.53 ± 0.11
IVSd, mm	1.74 ± 0.02	1.81 ± 0.01	1.77 ± 0.01	1.77 ± 0.01
LVPWTd, mm	1.74 ± 0.02	1.81 ± 0.01	1.77 ± 0.01	1.77 ± 0.01
IVSs, mm	2.78 ± 0.02	2.67 ± 0.05	2.82 ± 0.01	2.81 ± 0.01
LVPWs, mm	2.78 ± 0.02	2.67 ± 0.05	2.82 ± 0.05	2.80 ± 0.04
LVFS, %	41.75 ± 0.53	40.51 ± 0.60	41.98 ± 0.46	41.68 ± 0.65
LVEF, %	80.20 ± 0.53	78.89 ± 0.67	80.44 ± 0.46	80.11 ± 0.65
LVr/h	2.22 ± 0.06	2.26 ± 0.03	2.25 ± 0.05	2.19 ± 0.04
RG (n = 10)				
Heart rate	331.16 ± 10.23	294.10 ± 3.74***	296.50 ± 6.06	302.00 ± 4.98
LVEDD, mm	7.66 ± 0.14	8.59 ± 0.16*	8.72 ± 0.22*	8.90 ± 0.24***
LVESD, mm	4.36 ± 0.77	6.18 ± 0.18****	6.01 ± 0.33**	6.14 ± 0.37***
IVSd, mm	1.77 ± 0.02	1.53 ± 0.03****	1.47 ± 0.07***	1.48 ± 0.07***
LVPWTd, mm	1.77 ± 0.02	1.75 ± 0.02**	1.51 ± 0.04****	1.51 ± 0.05***
IVSs, mm	2.79 ± 0.04	2.06 ± 0.07****	2.19 ± 0.15**	2.27 ± 0.15***
LVPWs, mm	2.79 ± 0.04	2.32 ± 0.07***	2.27 ± 0.30**	2.22 ± 0.47***
LVFS, %	43.09 ± 0.41	28.06 ± 1.53****	31.39 ± 2.14***	31.55 ± 2.27***
LVEF, %	81.55 ± 0.39	62.31 ± 2.39****	66.07 ± 3.57***	66.96 ± 3.49***
LVr/h	2.17 ± 0.42	2.29 ± 0.07	2.93 ± 0.16**	3.01 ± 0.21**
N/S (n = 10)				
Heart rate	328.63 ± 6.57	329.37 ± 6.20†††	342.90 ± 8.84	351.43 ± 4.97
LVEDD, mm	7.66 ± 0.16	8.96 ± 0.24***	9.17 ± 0.22***	9.33 ± 0.22****
LVESD, mm	4.46 ± 0.11	6.78 ± 0.26****†	7.16 ± 0.33****††	7.52 ± 0.30****††
IVSd, mm	1.79 ± 0.02	1.37 ± 0.06****††	1.31 ± 0.06****†	1.24 ± 0.05****†††
LVPWTd, mm	1.79 ± 0.02	1.69 ± 0.01****†	1.37 ± 0.04****††	1.30 ± 0.04****††
IVSs, mm	2.83 ± 0.04	1.78 ± 0.11****†	1.83 ± 0.15****†	1.66 ± 0.13****†††
LVPWs, mm	2.83 ± 0.04	2.31 ± 0.04***	1.97 ± 0.32****†	1.78 ± 0.38****†††
LVFS, %	41.81 ± 0.45	24.38 ± 1.77****†	22.29 ± 2.01****†††	19.58 ± 1.82****††††
LVEF, %	80.27 ± 0.46	56.20 ± 3.02****	52.24 ± 3.51****†††	47.30 ± 3.36****†††
LVr/h	2.14 ± 0.045	2.52 ± 0.09*†	3.38 ± 0.16****†	3.63 ± 0.17****††

LVEDD, left ventricular end diastolic dimension; LVESD, left ventricular end systolic dimension; IVSs, intraventricular septum systole; IVSd, intraventricular septum diastole; LVPWTs, left ventricular posterior wall thickness systole; LVPWTd, left ventricular posterior wall thickness diastole; LVFS, left ventricular fractional shortening; LVEF, left ventricular ejection fraction; LVr/h, LV radius to PWTd ratio; d, days post-MI. Values in mean ± SE (SEM), *$P < 0.05$, **$P < 0.01$, ***$P < 0.001$, ****$P < 0.0001$ vs. Sham, †$P < 0.05$, ††$P < 0.01$, †††$P < 0.001$, ††††$P < 0.0001$ vs. RG.

presented in *Table 1*. In addition, analysis of variance with Bonferroni/Dunn post-hoc test repeated values analysis (echocardiography data) was used to compare the effects over time within the groups, and the *p* values are presented in Supporting Information, *Table S1*.

infarct/risk area ratio (%) between RG and N/S-treated rats. Quantification diagrams (*Figure 1C* and *D*) show infarct/risk area ratio (%) and infarct/all area ratio (%) between groups, respectively. The last is used as internal control of the method.

Results

RG improves cardiac function without altering infarct size

To determine whether RG could improve cardiac function, in a 28 days (post-MI) treatment model, echocardiography analysis was performed (*Table 1* and Supporting Information, *Table S1*). Baseline (pre-MI induction) measurements were similar in all groups. *Figure 1A* displays representative 2D targeted M-mode images. LVFS (%) was decreased both in RG and N/S-treated rats compared with Sham group at 7, 14, and 28 days post-MI induction (*Figure 1B* and *Table 1*). However, RG treatment diminished the increase in LV end-systolic diameter and consequently preserved the FS reduction compared with N/S-treated group at 14 days (31.4 ± 2.1 vs. 22.3 ± 2.0, $P < 0.0001$) and 28 days (31.6 ± 2.3 vs. 19.6 ± 1.8, $P < 0.0001$), respectively (*Table 1*). In addition, no significant difference was seen in the reduction of

RG attenuates fibrosis

Post-MI treatment with RG, for 28 days, clearly reduced (60.3%) interstitial fibrosis in the BZ (0.46 ± 0.27, *Figure 2B*) compared with N/S-treated group (1.16 ± 0.16) (*Figure 2C*) as evaluated by immunofluorescence staining of frozen cardiac tissue sections for collagen-αI, while, interstitial fibrosis on RR cardiac tissue sections did not reveal any difference between groups (data not shown). Desmin staining also indicated less cardiomyocyte damage in RG-treated group (*Figure 2B*). Furthermore, fibrosis assay analysis by myocardial HOP assay (*Figure 2E*) revealed that 28 days post-MI, RG treatment decreased myocardial fibrosis in the BZ compared with N/S-treated rats (1.34 ± 0.34 vs. 2.32 ± 0.29, $P < 0.05$). There was no statistical significant difference for the RR (0.98 ± 0.28 vs. 1.22 ± 0.15) between these two groups (*Figure 2E*).

The mRNA expression levels of the collagen type I in the BZ were increased in RG compared with N/S-treated group (7.06 ± 1.58 vs. 3.15 ± 0.57, $P < 0.05$), (*Figure 2F*). There

Figure 1 Rasagiline mesylate (RG) improves cardiac dysfunction at 14 and 28 days post-MI induction, without altering infarct size. (A) Representative 2D targeted M-mode images from the short axis view. (B) RG diminished the decrease in FS compared with N/S-treated group at 14 and 28 days ($P < 0.0001$). (C) Quantification diagram of infarct/risk area ratio (I/R %) and (D) Risk/all area ratio (%) as internal control of the method. *$P < 0.001$, **$P < 0.0001$ vs. Sham and †$P < 0.001$, ††$P < 0.0001$ vs. RG.

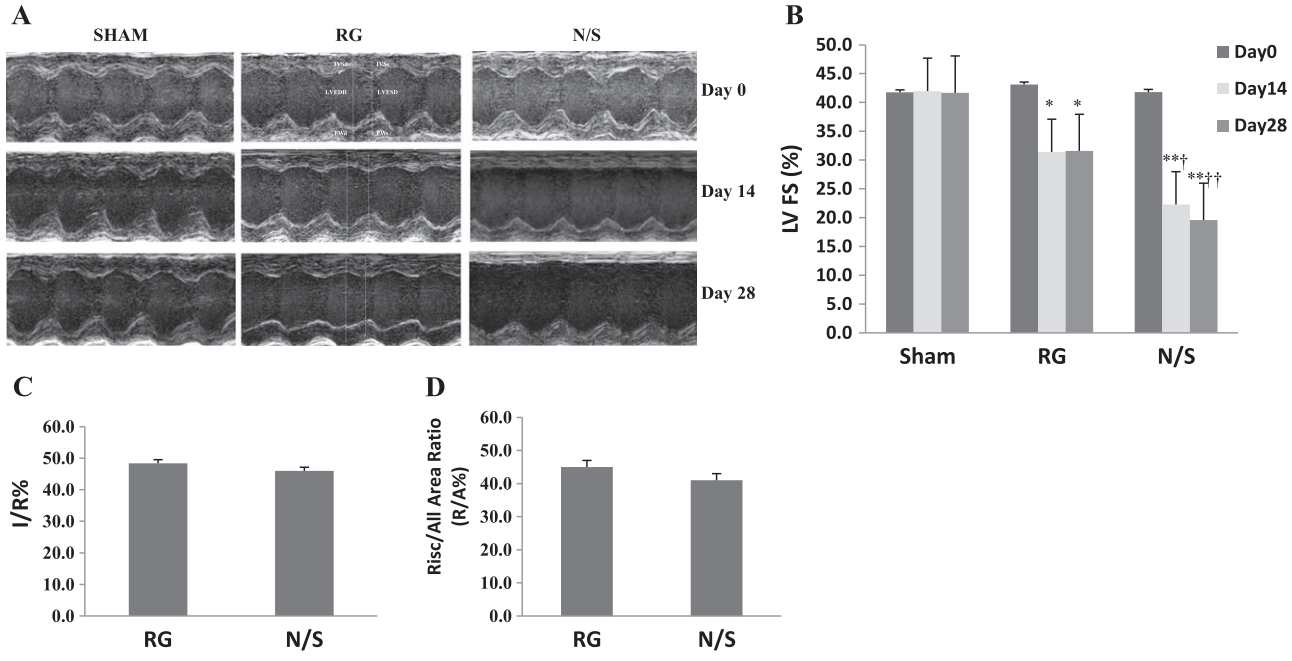

DOI: 10.1002/ehf2.12140

Figure 2 Interstitial fibrosis was evaluated by immunofluorescence staining of BZ tissue sections (green = desmin, red = collagen-αI, bar = 25 μm). (A) Sham group. (B) RG showed decreased interstitial fibrosis compared with N/S group (C). (D) Quantification diagram of collagen score between groups ($P < 0.05$ vs. N/S). (E) Fibrosis assay analysis showed that in the BZ, RG treatment decreased myocardial hydroxyproline concentration compared with N/S group ($P < 0.05$, $n = 5$). (F) Quantification diagrams showing variations in mRNA relative expression of TGF-β1, TIMP-2, and collagen type I genes in the BZ and (G) RR between groups ($n = 5$). Values are mean ± SE, $^{*}P < 0.05$, $^{**}P < 0.01$ vs. N/S.

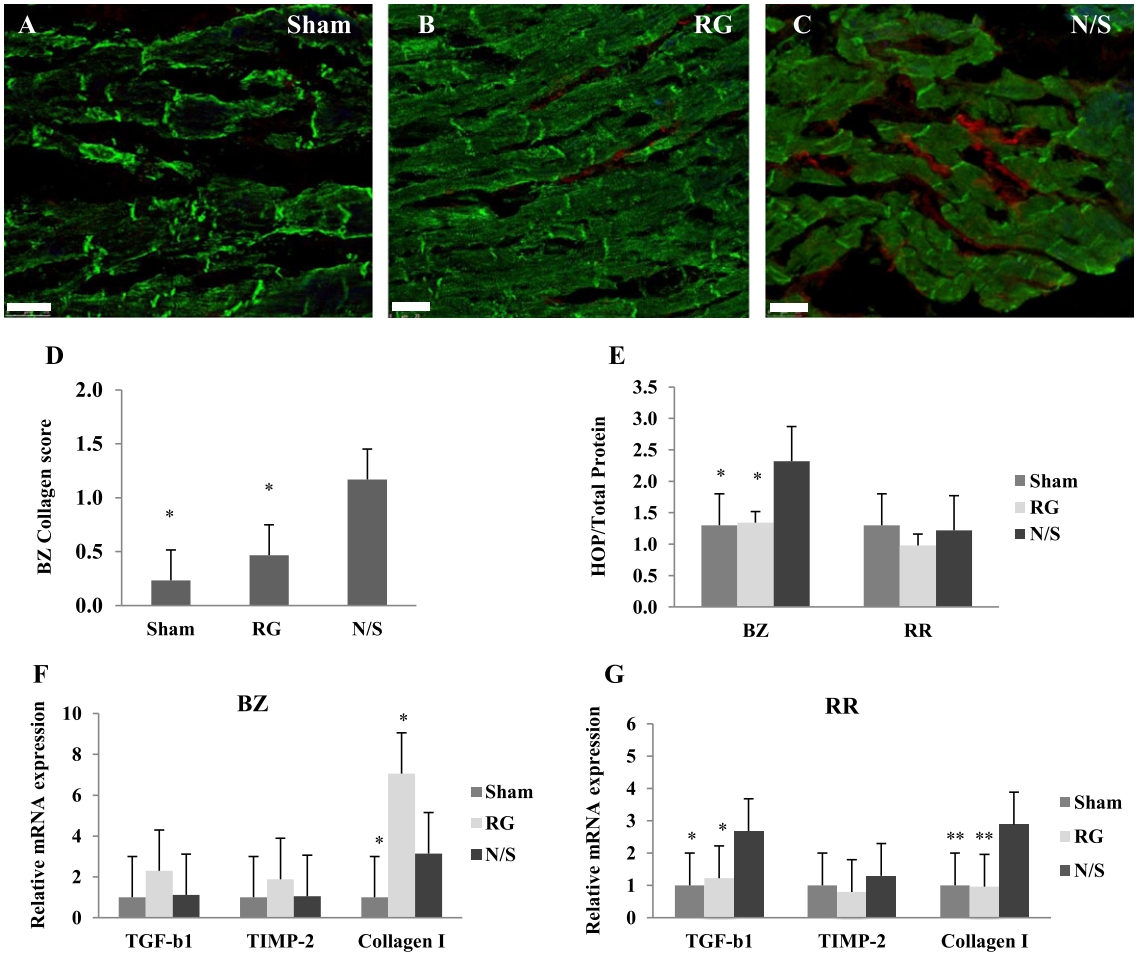

was no difference for TIMP-2 and TGF-b1 mRNA expression levels in the BZ for the above two groups (*Figure 2F*). In the RR, collagen type I (0.96 ± 0.17 vs. 2.89 ± 0.65, $P < 0.001$) and TGF-b1 (1.22 ± 0.28 vs. 2.68 ± 0.81, $P < 0.05$) mRNA expression levels were decreased in RG compared with N/S-treated rats (*Figure 2G*). MMP-2 mRNA expression levels were beyond the detection limit of the method in all samples analysed (data not shown).

RG attenuates apoptosis and cell death

To determine whether RG may attenuate the apoptotic cascade, we investigated by western blot analysis the protein levels of the pro apoptotic proteins Caspase 3 and Bax and the anti apoptotic protein Bcl-2. As shown in *Figure 3A*, the relative protein expression of cleaved caspase 3 was significantly attenuated by RG in the RR compared with N/S-treated group (0.72 ± 0.06 vs. 1.37 ± 0.11, $P < 0.001$). There was no statistical significant difference either for caspase 3 in the BZ or Bcl-2 and Bax protein levels in the RR or BZ (*Figure 3A* and *B*). The protein levels were normalized to GAPDH levels as indicated by representative Western immunoblots in *Figure 3C*. In order to further investigate the potential anti-apoptotic effect of RG treatment, apoptotic myocytes were calculated by TUNEL assay and connexin-43 staining of cardiomyocytes. RG treatment attenuated by 65% the number of apoptotic myocytes in the BZ compared with N/S group (0.53 ± 0.19 vs. 1.46 ± 0.30, *Figure 3D*). Representative TUNEL assay immunofluorescence staining of the BZ is depicted in *Figure 3E–G*.

DOI: 10.1002/ehf2.12140

Figure 3 The relative protein expression levels of Caspase 3, Bax, and Bcl2 were estimated by Western blot in RR (A) and BZ (B). (C) Representative western blot images are depicted. Cleaved Caspase 3 protein levels were diminished in the RR of the RG compared with N/S group ($P < 0.0001$, $n = 5$). (D) TUNEL quantification showed a significant reduction of apoptotic myocytes by 65% in the BZ of RG compared with N/S group ($P < 0.05$, $n = 5$). Values in mean ± SE, *$P < 0.05$, **$P < 0.0001$ vs. N/S. Representative images of BZ tissue sections from sham (E), RG (F), and N/S (G) group were stained for TUNEL nuclei (red), connexin-43 (green), and DAPI (blue). Bar 50 μm.

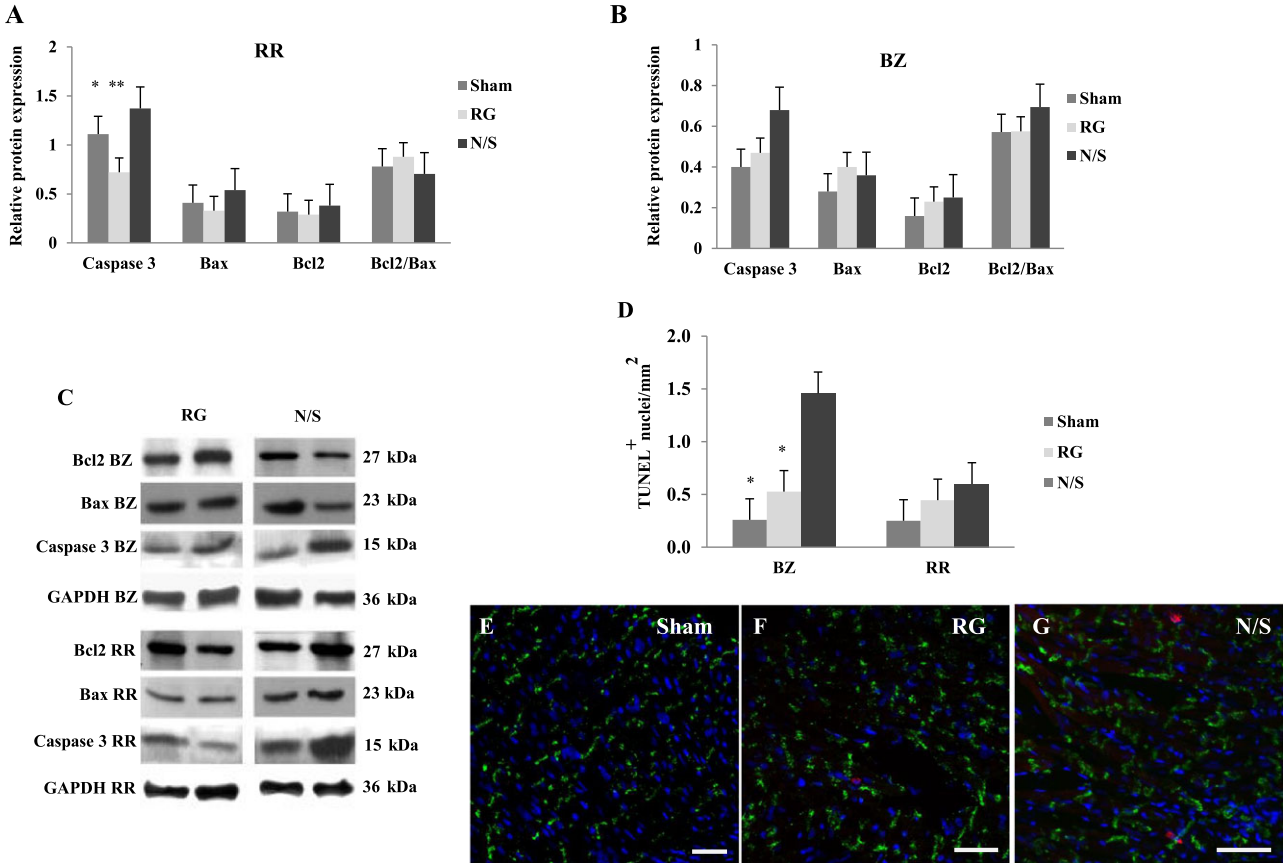

RG attenuates the increase in tissue oxidative stress

MDA levels were decreased in the BZ of RG compared with N/S-treated group (0.29 ± 0.02 vs. 0.53 ± 0.05, $P < 0.001$, *Figure 4A*). However, almost similar MDA levels were calculated in the RR in both groups (0.50 ± 0.08 vs. 0.45 ± 0.08, respectively). MDA levels for sham-operated rats were 0.42 ± 0.01 for the BZ and 0.57 ± 0.01 for the RR, respectively. In addition, there was a trend for increased small ubiquitin-related modifier 1 (SUMO-1) protein levels in both the BZ (2.32 ± 1.8 vs. 1.33 ± 0.88) and RR (2.67 ± 2.4 vs. 2.16 ± 1.84) of RG compared with N/S-treated group, but without statistical significance (*Figure 4B*).

Discussion

In the present study, we investigated the cardioprotective action of RG, a MAO-B inhibitor[16] with no adverse cardiovascular effects,[17] in a rat MI model of permanent ligation. Our study revealed a significant attenuation in post-MI LVR, characterized by reduced LV dilation preserving FS at 7, 14, and 28 days post-MI in RG-treated rats, accompanied by less BZ fibrosis and cardiomyocyte apoptosis, indicating a potential therapeutic impact of RG.

Several studies have demonstrated that both RG and its S-isomer TVP1022 have cardioprotective effects.[14,32] Most experimental studies provide TVP1022 before MI induction presenting beneficial effects in post-MI period under different experimental conditions.[13–15] Furthermore, the administration of TVP1022, at the time of coronary artery occlusion, significantly improved cardiac function and reduced myocardial fibrosis given at an ischemia/reperfusion animal model, studied 8 weeks post-MI.[32] We decided to use RG starting one day after MI induction because many drugs are given after primary percutaneous coronary intervention for ST-segment elevation MI (STEMI) and/or thrombolysis.

In agreement with its cardioprotective efficacy, treatment with RG prevented LV interstitial collagen deposition at a

Figure 4 (A) MDA levels were estimated in tissue extracts from BZ and RR. RG diminished MDA levels in BZ compared with N/S group ($P < 0.001$, $n = 4$). (B) Western blot analysis showed variations in small ubiquitin-related modifier-1 relative protein expression levels from RG and N/S group in the BZ and RR ($n = 4$). Values in mean ± SE, $^{*}P < 0.05$, $^{**}P < 0.001$ vs. N/S.

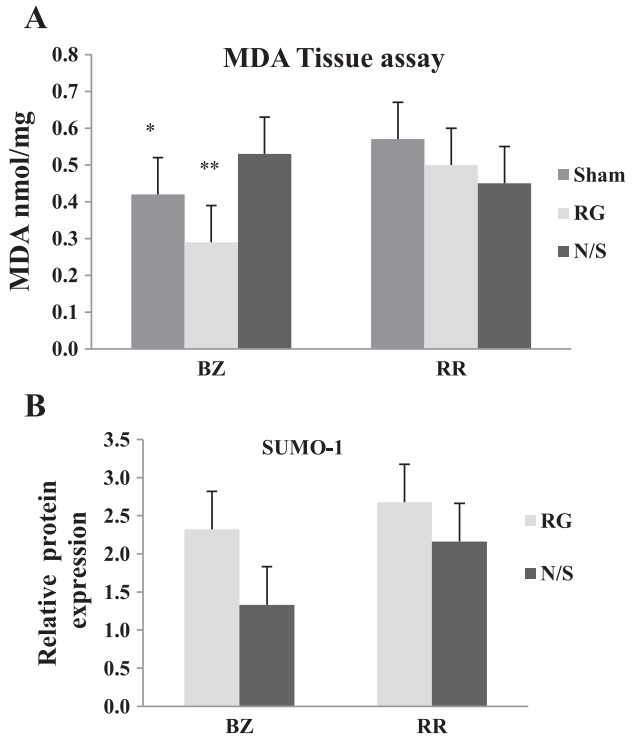

protein level (as indicated by immunofluorescence staining and HOP assay) and less cardiomyocyte degeneration was made evident by desmin staining[21] in the BZ. We also found that collagen type I mRNA levels were significantly increased in the BZ of the RG group. Changes in either synthesis or degradation may lead to heart failure. Preventing the breakdown of the extracellular collagen could arrest infarct expansion and eventually ventricular dilation.[33,34] Thus, we could hypothesize that RG treatment did not permit collagen mRNA to evolve into collagen protein formation (fibrosis), possibly by keeping fibroblasts in a viable state.

This observation also concurs with the significantly decreased relative mRNA levels of TGF-b and collagen type I in the RR of RG-treated rats. The cytokine TGF-b increases early in the infarct zone stimulating fibroblast proliferation. Moreover, tissue repair is initiated by the formation of a fibrin–fibronectin matrix, which precedes collagen synthesis. The treatment with RG revealed a preservation of the above mechanism 28 days post-MI in the RR, possibly by rescuing the injured myocytes and activating myocardial repair pathways. No significant difference was seen in the reduction of infarct/risk area ratio between RG and N/S-treated rats, and that could be attributed to the 24 h delay of RG treatment.

Furthermore, RG possesses anti-apoptotic properties either by the preservation of mitochondrial membrane potential[15] or by attenuating the expression of caspase 3.[14] Several studies also show that myocardial apoptosis in experimental MI models is elevated both in the BZ and RR as early as 24 h after MI in the infarct area and BZ[35,36] and up to 4 weeks post-MI in the RR.[37,38] In order to define the anti apoptotic effects of RG in this stable MI model, we performed TUNEL analysis which confirmed that RG attenuated the number of dead myocytes in BZ. To further support our data, we also explored caspase 3, an increasingly recognized modulator of cardiomyocyte apoptosis,[38] and Bcl-2/Bax ratio protein expression profile.

According to our findings, RG treatment demonstrated a reduction of activated Caspase 3 in the RR. It has been shown that in contrast to the BZ, the amount of apoptosis in the RR is correlated with an increase in the ventricular diameter 4 weeks after infarction.[37] More specifically, RG significantly preserved LVEDD and LVESD increased almost from 7 days post-MI in our study. This observation provides a possible association towards apoptosis in the RR which has previously been associated with post-infarction LVR, cardiac dilation, and increased cardiac fibrosis after MI, respectively.[37] In addition, we also observed a shift of the Bcl2/Bax ratio toward the regulator protein Bcl2 in the RR (although not statistically significant). This finding suggests at ischemic injury the increased expression of proapoptotic protein Bax and decreased expression of antiapoptotic protein Bcl-2 induces procaspase-3 cleavage;[30] we believe that the RG administration either earlier or a higher dose would be more effective at a molecular level.

Another important mechanism which plays a key role in cardiomyocyte apoptosis is oxidative stress. MDA is one of the most widely used markers to assess this process.[31,39] MDA levels were markedly decreased in the BZ of the RG group 28 days post-MI. This finding is very interesting because monoamine oxidases have been characterized as a source of oxidants such as H_2O_2 and aldehyde intermediates in the myocardium.[4] It has also been shown that MAO regulates the lipid peroxidation and other changes leading to cell death through reactive oxygen species.[40] Inhibition of MAO-B results in reduced formation of H_2O_2 and aldehydes, two molecules that are known to stimulate mitochondrial and myocardial damage.[41] Furthermore, in context with oxidative stress, we also explored SUMO-1 which has been found to be highly relevant in the response to cellular stress and rescues SERCA2a ATPase (cardiac isoform of sarcoplasmic reticulum calcium ATPase) activity in heart failure.[42,43] In the present study, we observed a trend towards elevation in SUMO-1 relative protein levels both in the BZ and RR of RG-treated group. Consequently, a potential increase of SUMO-1 may contribute to the reduction of LV dilation after MI induction and related to the cardioprotective activity of RG.

We consider as limitations of the study the lack of echocardiography and hemodynamic data in the acute setting. Furthermore, we did not perform an electrophysiology study for heart rate evaluation. The heart rate appeared to be significantly lower within the RG group compared with baseline measurement (pre-MI induction) and to the other two groups at day 7 post-MI, although within the normal limits, respectively. Regarding the excessive catecholaminergic increase in the early stages of heart failure and that the increase in heart rate is detrimental for cardiomyocytes in the long term, we believe that further investigation is required.

Taking into account that a failing heart is characterized by complex tissue remodeling involving increased cardiomyocyte death, impairment of sarcomere function and metabolic activity, together with increased inflammation and interstitial fibrosis.[3] Several studies have revealed that MAO inhibition is beneficial in cardiovascular pathologies. MAOs are able to trigger different signaling pathways leading to proliferation, apoptosis, or cell death, respectively.[4] The potential of their inhibition in the heart during chronic neuro-hormonal or hemodynamic stress can be directly associated with MAO-derived H_2O_2 and oxidative stress[40,41] or apoptosis reduction as well as mitochondrial viability either through Bcl2 and protein kinase C activation or Bax and caspase-3 down-regulation.[8,10,12,16] According to our findings we believe that RG preserved myocardial performance through several signaling pathways targeting oxidative stress, cardiomyocyte apoptosis, and favourable matrix remodeling.

In conclusion, our study revealed the potential effect of RG treatment in the post-MI period concerning the reduction in the progressive LV dilation, apoptosis, and oxidative stress. Additional studies are required to verify the protective effects of RG in LVR and to define MAO-B as a pharmacological therapeutic target.

Acknowledgements

We thank Dr Davos Constantinos, MD, PhD, Cardiologist (BRFAA) for his valuable comments on echocardiography study and Mr. Efentaki Panagioti, MSc for his help with scar size experiments (Pharmacology Department, National and Kapodistrian University of Athens).

Conflict of interest

None declared.

Funding

This work was supported by Olayan Investment group.

Supporting information

Supporting information may be found in the online version of this article.

Table S1. ANOVA/ Bonferroni/ Dunn post hoc test repeated measures analysis within groups.

References

1. Foley PW, Chalil S, Khadjooi K, Irwin N, Smith RE, Leyva F. Left ventricular reverse remodelling, long-term clinical outcome, and mode of death after cardiac resynchronization therapy. *Eur J Heart Fail* 2011; **13**: 43–51.
2. Burchfield JS, Xie M, Hill JA. Pathological ventricular remodeling: mechanisms: part 1 of 2. *Circulation* 2013; **128**: 388–400.
3. Tarone G, Balligand JL, Bauersachs J, Clerk A, De Windt L, Heymans S, Hilfiker-Kleiner D, Hirsch E, Iaccarino G, Knöll R, Leite-Moreira AF, Lourenço AP, Mayr M, Thum T, Tocchetti CG. Targeting myocardial remodeling to develop novel therapies for heart failure: a position paper from the Working Group on Myocardial Function of the European Society of Cardiology. *Eur J Heart Fail* 2014; **16**: 494–508.
4. Kaludercic N, Carpi A, Menabò R, Di Lisa F, Paolocci N. Monoamine oxidases (MAO) in the pathogenesis of heart failure and ischemia/reperfusion injury. *Biochim Biophys Acta* 1813; **2011**: 1323–1332.
5. Cheng Z, Ou L, Liu Y, Liu X, Li F, Sun B, Che Y, Kong D, Yu Y, Steinhoff G. Granulocyte colony-stimulating factor exacerbates cardiac fibrosis after myocardial infarction in a rat model of permanent occlusion. *Cardiovasc Res* 2008; **80**: 425–434.
6. Pfister O, Lorenz V, Oikonomopoulos A, Xu L, Häuselmann SP, Mbah C, Kaufmann BA, Liao R, Wodnar-Filipowicz A, Kuster GM. FLT3 activation improves post-myocardial infarction remodeling involving a cytoprotective effect on cardiomyocytes. *J Am Coll Cardiol* 2014; **63**: 1011–1019.
7. Pistacchi M, Martinello F, Gioulis M, Zambito MS. Rasagiline and rapid symptomatic motor effect in Parkinson's disease: review of literature. *Neurol Ther* 2013; **3**: 41–66.
8. Maruyama W, Yamamoto T, Kitani K, Carrillo MC, Youdim M, Naoi M. Mechanism underlying anti-apoptotic activity of a (−)deprenyl-related propargylamine, rasagiline. *Mech Ageing Dev* 2000; **116**: 181–191.
9. Youdim MB, Gross A, Finberg JP. Rasagiline [N-propargyl-1R(+)-aminoindan], a selective and potent inhibitor of mitochondrial monoamine oxidase B. *Br J Pharmacol* 2001; **132**: 500–506.
10. Mandel S, Weinreb O, Amit T, Youdim MB. Mechanism of neuroprotective action of the anti-Parkinson drug rasagiline and its derivatives. *Brain Res Brain Res Rev* 2005; **48**: 379–387.
11. Siderowf A, Stern M. Clinical trials with rasagiline: evidence for short-term and long-term effects. *Neurology* 2006; **66**: S80–S88.
12. Maruyama W, Akao Y, Carrillo MC, Kitani K, Youdium MB, Naoi M. Neuroprotection by propargylamines in Parkinson's disease: suppression of apoptosis and induction of prosurvival genes. *Neurotoxicol Teratol* 2002; **24**: 675–682.
13. Kleiner Y, Bar-Am O, Amit T, Berdichevski A, Liani E, Maor G, Reiter

I, Youdim MB, Binah O. TVP1022 and propargylamine protect neonatal rat ventricular myocytes against doxorubicin-induced and serum starvation-induced cardiotoxicity. *J Cardiovasc Pharmacol* 2008; **52**: 268–277.
14. Abassi ZA, Barac YD, Kostin S, Roguin A, Ovcharenko E, Awad H, Blank A, Bar-Am O, Amit T, Schaper J, Youdim M, Binah O. TVP1022 attenuates cardiac remodeling and kidney dysfunction in experimental volume overload-induced congestive heart failure. *Circ Heart Fail* 2011; **4**: 463–473.
15. Ertracht O, Liani E, Bachner-Hinenzon N, Bar-Am O, Frolov L, Ovcharenko E, Awad H, Blum S, Barac Y, Amit T, Adam D, Youdim M, Binah O. The cardioprotective efficacy of TVP1022 in a rat model of ischaemia/reperfusion. *Br J Pharmacol* 2011; **163**: 755–769.
16. Abassi ZA, Binah O, Youdim MB. Cardiovascular activity of rasagiline, a selective and potent inhibitor of mitochondrial monoamine oxidase B: comparison with selegiline. *Br J Pharmacol* 2004; **143**: 371–378.
17. Mendzelevski B, Sprenger CR, Spiegelstein O, Rabinovich-Guilatt L. Cardiac safety of rasagiline, a selective monoamine oxidase type B inhibitor for the treatment of Parkinson's disease: a thorough QT/QTc study. *Int J Clin Pharmacol Ther* 2014; **52**: 192–201.
18. Union E. Directive 2010/63 on the protection of animals used for scientific purposes. *O J EUL* 2010; **276**: 33–79.
19. Speiser Z, Mayk A, Eliash S, Cohen S. Studies with rasagiline, a MAO-B inhibitor, in experimental focal ischemia in the rat. *J Neural Transm* 1999; **106**: 593–606.
20. Carrillo MC, Minami C, Kitani K, Maruyama W, Ohashi K, Yamamoto T, Naoi M, Kanai S, Youdim MB. Enhancing effect of rasagiline on superoxide dismutase and catalase activities in the dopaminergic system in the rat. *Life Sci* 2000; **67**: 577–585.
21. Psarras S, Mavroidis M, Sanoudou D, Davos CH, Xanthou G, Varela AE, Panoutsakopoulou V, Capetanaki Y. Regulation of adverse remodelling by osteopontin in a genetic heart failure model. *Eur Heart J* 2012; **33**: 1954–1963.
22. Morgan EE, Faulx MD, McElfresh TA, Kung TA, Zawaneh MS, Stanley WC, Chandler MP, Hoit BD. Validation of echocardiographic methods for assessing left ventricular dysfunction in rats with myocardial infarction. *Am J Physiol Heart Circ Physiol* 2004; **287**: H2049–H2053.
23. Masuda K, Taenaka H, Asanuma T, Nakatani S. Comparison of the effects of angiotensin II receptor antagonist monotherapy and combination therapy with a diuretic on cardiac function in spontaneously hypertensive rats. *J Echocardiogr* 2012; **10**: 125–131.
24. Gao S, Ho D, Vatner DE, Vatner SF. Echocardiography in mice. *Curr Protoc Mouse Biol* 2011; **1**: 71–83.
25. Tseliou E, Pollan S, Malliaras K, Terrovitis J, Sun B, Galang G, Marbán L, Luthringer D, Marbán E. Allogeneic cardiospheres safely boost cardiac function and attenuate adverse remodeling after myocardial infarction in immunologically mismatched rat strains. *J Am Coll Cardiol* 2013; **61**: 1108–1119.
26. Pantos C, Mourouzis I, Galanopoulos G, Gavra M, Perimenis P, Spanou D, Cokkinos DV. Thyroid hormone receptor alpha1 downregulation in postischemic heart failure progression: the potential role of tissue hypothyroidism. *Horm Metab Res* 2010; **42**: 718–724.
27. Bibli SI, Andreadou I, Chatzianastasiou A, Tzimas C, Sanoudou D, Kranias E, Brouckaert P, Coletta C, Szabo C, Kremastinos DT, Iliodromitis EK, Papapetropoulos A. Cardioprotection by H2S engages a cGMP-dependent protein kinase G/phospholamban pathway. *Cardiovasc Res* 2015; **106**: 432–442.
28. Prockop DJ, Udenfriend S. A specific method for the analysis of hydroxyproline in tissues and urine. *Anal Biochem* 1960; **1**: 228–239.
29. Pucheu S, Coudray C, Vanzetto G, Favier A, Machecourt J, de Leiris J. Assessment of radical activity during the acute phase of myocardial infarction following fibrinolysis: utility of assaying plasma malondialdehyde. *Free Radic Biol Med* 1995; **19**: 873–881.
30. Bianchi P, Kunduzova O, Masini E, Cambon C, Bani D, Raimondi L, Seguelas MH, Nistri S, Colucci W, Leducq N, Parini A. Oxidative stress by monoamine oxidase mediates receptor-independent cardiomyocyte apoptosis by serotonin and postischemic myocardial injury. *Circulation* 2005; **112**: 3297–3305.
31. Livak KJ, Schmittgen TD. Analysis of relative gene expression data using real-time quantitative PCR and the 2(−Delta Delta C(T)). *Methods* 2001; **25**: 402–408.
32. Malka A, Meerkin D, Barac YD, Malits E, Bachner-Hinenzon N, Carasso S, Ertracht O, Angel I, Shofti R, Youdim M, Abassi Z, Binah O. TVP1022: a novel cardioprotective drug attenuates left ventricular remodeling after ischemia/reperfusion in pigs. *J Cardiovasc Pharmacol* 2015; **66**: 214–222.
33. Sutton MG, Sharpe N. Left ventricular remodeling after myocardial infarction: pathophysiology and therapy. *Circulation* 2000; **101**: 2981–2988.
34. Zile MR, Brutsaert DL. New concepts in diastolic dysfunction and diastolic heart failure: Part II: causal mechanisms and treatment. *Circulation* 2002; **105**: 1503–1508.
35. Backlund T, Palojoki E, Saraste A, Eriksson A, Finckenberg P, Kyto V, Lakkisto P, Mervaala E, Voipio-Pulkki LM, Laine M, Tikkanen I. Sustained cardiomyocyte apoptosis and left ventricular remodelling after myocardial infarction in experimental diabetes. *Diabetologia* 2004; **47**: 325–330.
36. Abbate A, Morales C, De Falco M, Fedele V, Biondi Zoccai GG, Santini D, Palleiro J, Vasaturo F, Scarpa S, Liuzzo G, Severino A, Baldi F, Crea F, Biasucci LM, Vetrovec GW, Gelpi RJ, Baldi A. Ischemia and apoptosis in an animal model of permanent infarct-related artery occlusion. *Int J Cardiol* 2007; **121**: 109–111.
37. Palojoki E, Saraste A, Eriksson A, Pulkki K, Kallajoki M, Voipio-Pulkki LM, Tikkanen I. Cardiomyocyte apoptosis and ventricular remodeling after myocardial infarction in rats. *Am J Physiol Heart Circ Physiol* 2001; **280**: H2726–H2731.
38. Schwarz K, Simonis G, Yu X, Wiedemann S, Strasser RH. Apoptosis at a distance: remote activation of caspase-3 occurs early after myocardial infarction. *Mol Cell Biochem* 2006; **281**: 45–54.
39. Rodrigo R, Libuy M, Feliú F, Hasson D. Oxidative stress-related biomarkers in essential hypertension and ischemia–reperfusion myocardial damage. *Dis Markers* 2013; **35**: 773–790.
40. Mialet-Perez J, Bianchi P, Kunduzova O, Parini A. New insights on receptor-dependent and monoamine oxidase-dependent effects of serotonin in the heart. *J Neural Transm* 2007; **114**: 823–827.
41. Kaludercic N, Carpi A, Nagayama T, Sivakumaran V, Zhu G, Lai EW, Bedja D, De Mario A, Chen K, Gabrielson KL, Lindsey ML, Pacak K, Takimoto E, Shih JC, Kass DA, Di Lisa F, Paolocci N. Monoamine oxidase B prompts mitochondrial and cardiac dysfunction in pressure overloaded hearts. *Antioxid Redox Signal* 2014; **20**: 267–280.
42. Kho C, Lee A, Jeong D, Oh JG, Chaanine AH, Kizana E, Park WJ, Hajjar RJ. SUMO1-dependent modulation of SERCA2a in heart failure. *Nature* 2011; **477**: 601–605.
43. Lee A, Jeong D, Mitsuyama S, Oh JG, Liang L, Ikeda Y, Sadoshima J, Hajjar RJ, Kho C. The role of SUMO-1 in cardiac oxidative stress and hypertrophy. *Antioxid Redox Signal* 2014; **21**: 1986–2001.